

One-loop effects of MSSM particles in $e^-e^+ \rightarrow Zh$ and $e^-e^+ \rightarrow \nu\bar{\nu}h$ at the ILC

Yusaku Kouda^{1,*}, Tadashi Kon¹, Yoshimasa Kurihara², Tadashi Ishikawa²,
Masato Jimbo³, Kiyoshi Kato⁴ and Masaaki Kuroda⁵

¹ Seikei University, Musashino, Tokyo 180-8633, Japan

* E-mail: dd146101@cc.seikei.ac.jp

² KEK, Tsukuba, Ibaraki 305-0801, Japan

³ Chiba University of Commerce, Ichikawa, Chiba 272-8512, Japan

⁴ Kogakuin University, Shinjuku, Tokyo 163-8677, Japan

⁵ Meiji Gakuin University, Yokohama, Kanagawa 244-8539, Japan

Abstract

The 1-loop effects of the MSSM at the ILC are investigated through numerical analysis. We studied the higgs production processes $e^-e^+ \rightarrow Zh$ and $e^-e^+ \rightarrow \nu\bar{\nu}h$ at the ILC. It is found that the magnitude of the MSSM contribution through the 1-loop effects is sizable enough to be detected. In the study, three sets of the MSSM parameters are proposed, which are consistent with the observed higgs mass, the muon $g-2$, the dark matter abundance and the decay branching ratios of B mesons. In the $e^-e^+ \rightarrow Zh$ process, the 1-loop effects of the MSSM are visible and the distinction of the parameter sets is partially possible. For the study of $e^-e^+ \rightarrow \nu\bar{\nu}h$, we used the equivalent W -boson approximation in the evaluation of the 1-loop cross section. While the 1-loop effect of the MSSM is visible, the distinction of the parameter sets might not be possible in this process under the value of realistic luminosity at the ILC.

1 Introduction

The standard model (SM) is completed by the discovery of the last piece, the higgs particle. However, it is argued that it is not the final theory of the fundamental particles. For example, the SM includes a lot of free parameters. When one calculates the mass of higgs, the values of these parameters are intentionally selected to cancel the quantum correction. This cancellation is as precise as up to around 17 order. Some researchers regard it as “unnatural”.

The supersymmetric (SUSY) model [1] is considered as one of the promising candidates for the theory beyond the standard model. In this theory, each particle in the SM has its supersymmetric partner, or, a sparticle. The quadratic divergence in the calculation of quantum correction to the higgs mass is canceled by other contributions from the sparticles, so that the fine tuning problem disappears. The search of sparticles is the important subject of the present and future collider experiments to prove the SUSY. In spite of hard efforts in the large hadron collider (LHC) experiments, slightest signature of their existence has not been obtained. For example, the scalar top particle (stop) seems not to exist under $\mathcal{O}(1)$ TeV mass region [2, 3]. Though sparticles are so heavy that it is difficult to be produced directly, the indirect signature would be expected at the international linear collider (ILC).

Since high luminosity is expected at the ILC experiments [4], the quite small experimental error is expected. Correspondingly, therefore, the quite accurate calculations of the physical observables are required. As an explicit model, the Minimal Supersymmetric Standard Model (MSSM) is studied in this paper. We have calculated cross sections and decay branching ratios at the 1-loop level using the GRACE/SUSY-loop system [5, 6, 7, 8, 9]. In this paper we report numerical results on the cross section of $e^-e^+ \rightarrow Zh$ [10]. Our results are consistent with those given in the previous work [11] under the same setting of MSSM parameters. We have also calculated the cross section of $e^-e^+ \rightarrow \nu\bar{\nu}h$, with the equivalent W -boson approximation (EWA) [12]. The complete SM 1-loop correction of $\sigma(e^-e^+ \rightarrow Zh)$ and $\sigma(e^-e^+ \rightarrow \nu\bar{\nu}h)$ have already been calculated using the GRACE [13] and we reproduced the results for comparison. We calculate the MSSM 1-loop correction to perform the indirect search of sparticles as they contribute to the cross sections through 1-loop diagrams.

The parameter sets of the MSSM are chosen so as to meet the various experimental constraints. They

include the anomalous magnetic moment of muon $g-2$ [14, 15], the dark matter (DM) thermal relic density [16, 17, 18], B meson rare decay branching ratio $\text{Br}(b \rightarrow s\gamma)$ [19] and the higgs mass [20, 21]. By the constraints the mass spectra of MSSM are quite limited. For the selection of MSSM mass spectra we utilized the following program packages. `MicrOMEGAs` [22] was used in the estimation of the DM thermal relic density and `SuSpect2` [23] was used for $g-2$, $\text{Br}(b \rightarrow s\gamma)$ and m_h .

2 The selection of the MSSM parameter sets

In Table 1 we show experimental constraints we have considered, and in Table 2 we show three MSSM parameter sets we have selected. Detailed methods for the selection of sets have been explained in the previous work [6].

The first common settings in the three sets are

(A) $M_1 = 350\text{GeV}$, $M_2 = 450\text{GeV}$, $\mu = 1\text{TeV}$, $\tan\beta = 50$ and $m_{\tilde{\ell}} < 500\text{GeV}$ ($\ell = e, \mu$).

They are necessary for sets to satisfy the constraints (1), (2) and (3) in Table.1. As a consequence, the lightest sparticle (LSP) is almost Bino $\tilde{\chi}_1^0 \simeq \tilde{B}$ with mass about 350GeV , $m_{\tilde{\chi}_2^0} \simeq m_{\tilde{\chi}_1^+} \simeq 450\text{GeV}$ (almost Wino \tilde{W}) and $m_{\tilde{\chi}_{3,4}^0} \simeq m_{\tilde{\chi}_2^+} \simeq 1\text{TeV}$ (almost higgsino \tilde{H}). The second common settings are

(B) a large mass splitting in the stau $\tilde{\tau}$ sector, $m_{\tilde{\tau}_1} \simeq 365\text{GeV}$ ($\gtrsim m_{\tilde{\chi}_1^0}$), $m_{\tilde{\tau}_2} \simeq 554\text{GeV}$ and $m_{\tilde{\nu}_\tau} \simeq 466\text{GeV}$.

They are necessary for sets to be satisfied the constraint (4), because the co-annihilation occurring between $\tilde{\tau}_1$ and the LSP is required for meeting this constraint in the Bino LSP case. The difference among the three sets exists in the settings of masses of the strongly interacting sparticles ($m_{\tilde{g}} (= M_3)$ and $m_{\tilde{q}}$), gluino and squarks. Considering the LHC bounds (5), we take $(m_{\tilde{g}} \text{ and } m_{\tilde{q}}) \simeq (2\text{TeV}, 1.5\text{TeV})$, $(5\text{TeV}, 5\text{TeV})$ and $(10\text{TeV}, 10\text{TeV})$ for set 1, set 2 and set 3, respectively. For each set, the left-right mixing parameter θ_t and masses $m_{\tilde{t}_{1,2}}$ in the stop \tilde{t} sector are tuned to satisfy the higgs mass constraint (6).

Table 1: The experimental constraints for MSSM parameters.

	Experimental bounds
(1) muon $g-2$ anomalous magnetic moment [14]	$a_\mu^{\text{exp}} - a_\mu^{\text{SM}} = (2.88 \pm 0.63 \pm 0.49) \times 10^{-9}$
(2) B meson rare decay branching ratio [19]	$\text{Br}(B \rightarrow \chi_s \gamma) = (3.43 \pm 0.21 \pm 0.07) \times 10^{-4}$
(3) LHC direct search of chargino and neutralino [24][25]	$m_{\tilde{\chi}_1^0} \gtrsim 300$ GeV for $m_{\tilde{\chi}_1^\pm, \tilde{\chi}_2^0} = 500$ GeV
(4) DM thermal relic density [18]	$\Omega h^2 = 0.1198 \pm 0.0026$
(5) LHC direct search of gluino squark [26][27]	$m_{\tilde{g}}, m_{\tilde{q}} \gtrsim 1.5$ TeV
(6) higgs mass [20][21]	$m_h(\text{exp}) = 125.09 \pm 0.24$ GeV

Table 2: Masses and MSSM parameters for three sets (masses in unit of GeV)

set 1				set 2				set 3			
$\tilde{\chi}_1^+$	$\tilde{\chi}_2^+$			$\tilde{\chi}_1^+$	$\tilde{\chi}_2^+$			$\tilde{\chi}_1^+$	$\tilde{\chi}_2^+$		
456.2	1008			456.2	1008			456.2	1008		
$\tilde{\chi}_1^0$	$\tilde{\chi}_2^0$	$\tilde{\chi}_3^0$	$\tilde{\chi}_4^0$	$\tilde{\chi}_1^0$	$\tilde{\chi}_2^0$	$\tilde{\chi}_3^0$	$\tilde{\chi}_4^0$	$\tilde{\chi}_1^0$	$\tilde{\chi}_2^0$	$\tilde{\chi}_3^0$	$\tilde{\chi}_4^0$
349.2	456.2	1003	1007	349.2	456.3	1003	1007	349.2	456.2	1003	1007
$\tilde{\ell}_1$	$\tilde{\ell}_2$	$\tilde{\nu}_\ell$		$\tilde{\ell}_1$	$\tilde{\ell}_2$	$\tilde{\nu}_\ell$		$\tilde{\ell}_1$	$\tilde{\ell}_2$	$\tilde{\nu}_\ell$	
452.3	471.9	465.7		472.2	472.2	465.9		472.2	471.9	465.8	
$\tilde{\tau}_1$	$\tilde{\tau}_2$	$\tilde{\nu}_\tau$		$\tilde{\tau}_1$	$\tilde{\tau}_2$	$\tilde{\nu}_\tau$		$\tilde{\tau}_1$	$\tilde{\tau}_2$	$\tilde{\nu}_\tau$	
364.9	553.8	465.7		365.0	553.8	465.9		364.9	554.5	465.8	
\tilde{u}_1	\tilde{u}_2	\tilde{d}_1	\tilde{d}_2	\tilde{u}_1	\tilde{u}_2	\tilde{d}_1	\tilde{d}_2	\tilde{u}_1	\tilde{u}_2	\tilde{d}_1	\tilde{d}_2
1499	1500	1500	1501	5000	5000	5000	5000	10000	10000	10000	10000
\tilde{t}_1	\tilde{t}_2	\tilde{b}_1	\tilde{b}_2	\tilde{t}_1	\tilde{t}_2	\tilde{b}_1	\tilde{b}_2	\tilde{t}_1	\tilde{t}_2	\tilde{b}_1	\tilde{b}_2
1413	1593	1461	1539	4774	5220	4990	5010	9865	10130	9994	10010
θ_τ	θ_b	θ_t		θ_τ	θ_b	θ_t		θ_τ	θ_b	θ_t	
0.7969	0.7913	0.7840		0.8030	0.7912	0.7852		0.8010	0.7912	0.7853	
M_1	M_2	M_3		M_1	M_2	M_3		M_1	M_2	M_3	
350.0	450.0	2000		350.0	450.0	5000		350.0	450.0	10000	
$\mu=1000, \tan\beta=50$				$\mu=1000, \tan\beta=50$				$\mu=1000, \tan\beta=50$			

3 Calculation scheme

3.1 The GRACE system

There are more than twice as many different types of particles in the MSSM as those in the SM ; therefore, there are various possible sparticle production processes in the collider experiments. A large number of Feynman diagrams appearing in each production process requires tedious and lengthy calculations in evaluating the cross sections. Accurate theoretical prediction requires an automated system to manage such large scale computations. The **GRACE** system for the MSSM calculations[28, 9] has been developed by the KEK group (the Minami-tateya group) to meet the requirement. The **GRACE** system uses a renormalization prescription that imposes mass shell conditions on as many particles as possible, while maintaining the gauge symmetry by setting the renormalization conditions appropriately[9]. In the **GRACE** system for the SM, the usual 't Hooft-Feynman linear gauge condition is generalized to a more general non-linear gauge (NLG) that involves five extra parameters [29, 30]. We extend it to the MSSM formalism by adding the SUSY interactions with seven NLG parameters [9, 31]. We can check the consistency of the gauge symmetry by verifying the independence of the physical results from the NLG parameters. We ascertain that the results of the automatic calculation are reliable by carrying out the following checks:

- Electroweak (ELWK) non-linear gauge invariance check (NLG check)
- Cancellation check of ultraviolet divergence (UV check)
- Cancellation check of infrared divergence (IR check)
- Check of soft photon cut-off energy independence (k_c check)

Actually, the 1-loop differential cross sections (distributions) are separated into two parts,

$$d\sigma_{L\&S}^M(k_c) \equiv d\sigma_{\text{virtual}}^M + d\sigma_{\text{soft}}(k_c), \quad (1)$$

where the suffix M indicates SM or MSSM, and each part is computed separately. The loop and the counter term contribution $d\sigma_{\text{virtual}}^M$ should be gauge invariant and the UV finite but IR divergent. We regularize the IR divergence by the fictitious photon mass λ , so both $d\sigma_{\text{virtual}}^M$ and the soft photon contribution $d\sigma_{\text{soft}}$ are λ dependent. The λ dependence is canceled in $d\sigma_{L\&S}^M$. Finally, the k_c independent 1-loop physical cross sections can be obtained by

$$d\sigma_{1\text{loop}}^M \equiv d\sigma_{\text{tree}} + d\sigma_{L\&S}^M(k_c) + \int \int_{k_c} \frac{d\sigma_{\text{hard}}}{d\Omega dk}, \quad (2)$$

where, k and Ω are the energy and the solid angle of the photon respectively. We selected the values of the MSSM parameters related to the higgs sector so that the tree level cross section are numerically identical between the MSSM and the SM. Therefore, the suffix M can be neglected in $d\sigma_{\text{tree}}$ and $d\sigma_{\text{hard}}$. For the confirmation of the verifiability of 1-loop correction, we defined following correction ratios,

$$\delta_{\text{NLO}}^M \equiv \frac{d\sigma_{1\text{loop}}^M - d\sigma_{\text{tree}}}{d\sigma_{\text{tree}}}. \quad (3)$$

For the estimation of effects of the MSSM virtual particles, we defined following ratio [32],

$$\delta_{\text{susy}} \equiv \delta_{\text{NLO}}^{\text{MSSM}} - \delta_{\text{NLO}}^{\text{SM}} = \frac{d\sigma_{1\text{loop}}^{\text{MSSM}} - d\sigma_{1\text{loop}}^{\text{SM}}}{d\sigma_{\text{tree}}} = \frac{d\sigma_{L\&S}^{\text{MSSM}} - d\sigma_{L\&S}^{\text{SM}}}{d\sigma_{\text{tree}}}. \quad (4)$$

For the process $e^- e^+ \rightarrow Zh$, we calculated differential cross sections

$$d\sigma_{\text{tree,1loop}} = \left(\frac{d\sigma}{d \cos \theta_Z} \right)_{\text{tree,1loop}}, \quad (5)$$

where θ_Z is the scattering angle of the Z -boson.

3.2 Equivalent W -boson Approximation (EWA)

For the process $e^-e^+ \rightarrow \nu\bar{\nu}h$, we should calculate the cross section,

$$\sigma(s) \equiv \sum_{\ell=e,\mu,\tau} \sigma(e^-e^+ \rightarrow \nu_\ell\bar{\nu}_\ell h). \quad (6)$$

However, the estimation of the MSSM full 1-loop correction for (6) is difficult even using the **GRACE** system because the number of Feynman diagrams of the process $e^-e^+ \rightarrow \nu\bar{\nu}h$ becomes about 10^4 . In this paper, therefore, we use the EWA formulae [12],

$$\sigma'(s) \equiv \sum_{n=-1}^{+1} \int_{x_{min}}^1 f_n(x) \hat{\sigma}_n(\hat{s}) dx, \quad (7)$$

where $\hat{s} \equiv xs$ and $\hat{\sigma}_n(\hat{s})$ denotes the center of mass energy squared and cross section of the sub-process $e^-W_n^+ \rightarrow \nu_e h$. Then we set $x_{min} = (m_e + m_W)^2/s$. $f_n(x)$ are the energy distribution functions for W_n -boson with helicity $n = -1, 0, +1$,

$$f_0(x) = (g_L^2 + g_R^2) \left(\frac{x}{16\pi^2} \right) \left[\frac{2(1-x)\zeta}{\omega^2 x} - \frac{2\Delta(2-\omega)}{\omega^3} \ln \left(\frac{x}{\Delta'} \right) \right], \quad (8)$$

$$f_{+1}(x) = g_L^2 h_2 + g_R^2 h_1, \quad (9)$$

$$f_{-1}(x) = g_L^2 h_1 + g_R^2 h_2, \quad (10)$$

where

$$h_1 = \frac{x}{16\pi^2} \left[\frac{-(1-x)(2-\omega)}{\omega^2} + \frac{(1-\omega)(\zeta-\omega^2)}{\omega^3} \ln \left(\frac{1}{\Delta'} \right) - \frac{\zeta-2x\omega}{\omega^3} \ln \left(\frac{1}{x} \right) \right], \quad (11)$$

$$h_2 = \frac{x}{16\pi^2} \left[\frac{-(1-x)(2-\omega)}{\omega^2(1-\omega)} + \frac{\zeta}{\omega^3} \ln \left(\frac{x}{\Delta'} \right) \right], \quad (12)$$

$\omega = x - \Delta$, $\zeta = x + \Delta$, $\Delta = m_W^2/s$, $\Delta' = \Delta/(1-\omega)$. For the electron and W -boson coupling, $g_L = e/(\sqrt{2}\sin\theta_W)$ and $g_R = 0$. Moreover, the EWA cross section (7) is numerically indistinguishable

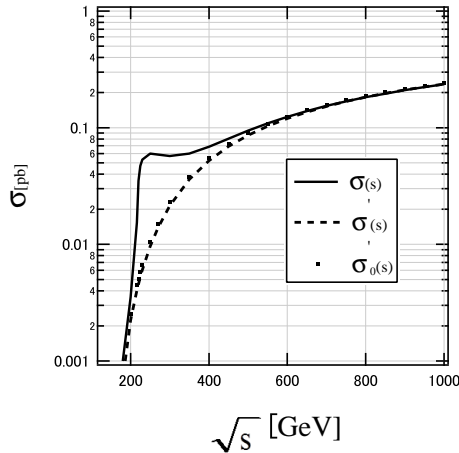


Figure 1: \sqrt{s} dependence of tree level total cross sections of $e^-e^+ \rightarrow \nu\bar{\nu}h$. The solid line and the dashed line and the dotted points correspond to σ , σ' and σ'_0 , respectively.

from

$$\sigma'_0(s) \equiv \int_{x_{min}}^1 f_0(x) \hat{\sigma}_0(\hat{s}) dx, \quad (13)$$

in the energy range considered here, because the contribution of W_{\pm} is almost negligible as shown in Figures.

In Figure 1, \sqrt{s} dependence of the tree level cross sections (6), (7) and (13) are shown. The cross section of $e^{-}e^{+} \rightarrow Zh \rightarrow \nu\bar{\nu}h$ is apparently large in the region $\sqrt{s} \lesssim 400\text{GeV}$. We calculated the differential cross section for $e^{-}e^{+} \rightarrow Zh$ at $\sqrt{s} = 250\text{GeV}$, where its total cross section has almost the largest value. On the other hand, the W -fusion contribution is dominant at $\sqrt{s} \gtrsim 500\text{GeV}$ and the EWA becomes good approximation. For example, $(\sigma - \sigma')/\sigma \simeq (-8.4, +0.75)\%$ and $(\sigma - \sigma'_0)/\sigma \simeq (-4.7, +3.2)\%$ at $\sqrt{s} = (500, 1000)\text{ GeV}$. We use σ'_0 for the calculation of cross sections at $\sqrt{s} = 500\text{GeV}$. We calculated the differential cross section,

$$d\sigma_{\text{tree,1loop}} = \left(\frac{d\sigma'_0}{dE_h} \right)_{\text{tree,1loop}}, \quad (14)$$

where E_h is the energy of higgs particle. It is calculated from (13) using relations

$$\frac{d\sigma'_0}{dE_h} = \frac{2x}{\sqrt{E_h^2 - m_h^2}} \frac{d\sigma'_0}{dx}, \quad (15)$$

$$x = \frac{1}{s} \left(E_h + \sqrt{E_h^2 - m_h^2} \right)^2. \quad (16)$$

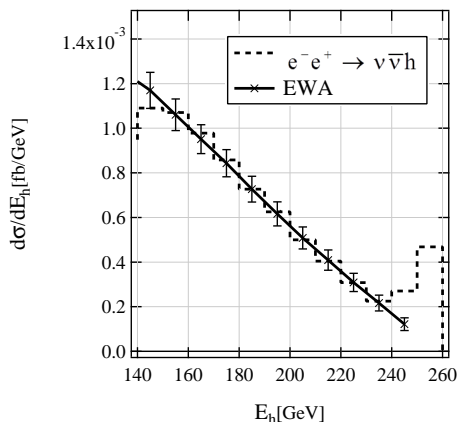


Figure 2: The higgs energy distribution at tree level of $e^{-}e^{+} \rightarrow \nu\bar{\nu}h$ (dotted), and that with EWA(solid). Here we assume $L = 500\text{ fb}^{-1}$.

In Figure 2, we show the tree level energy distribution of the higgs $d\sigma/dE_h$ from (6) and $d\sigma'_0/dE_h$ in (15) at $\sqrt{s}=500\text{ GeV}$. The statistical errors were calculated assuming $L=500\text{fb}^{-1}$. The difference is within the error range in the region $E_h=150\sim 230\text{ GeV}$. We could figure out that the EWA reproduce the $e^{-}e^{+} \rightarrow \nu\bar{\nu}h$ cross section in this energy region. The peak from Zh production around $E_h=250\text{ GeV}$ cannot be reproduced by the EWA.

4 The numerical results

4.1 The SM contribution

Table 3 shows the SM parameters which we used in the calculations. All the following numerical results (include the MSSM cross section) are computed in these parameters. Figure 3 shows the $\delta_{\text{NLO}}^{\text{SM}}$ in (3) for $e^{-}e^{+} \rightarrow Zh$ at $\sqrt{s}=250\text{ GeV}$ (left) and $e^{-}e^{+} \rightarrow \nu\bar{\nu}h$ used EWA at $\sqrt{s}=500\text{GeV}$ (right). The plotted errors were calculated assuming $L=250\text{ fb}^{-1}$ and 500 fb^{-1} for $e^{-}e^{+} \rightarrow Zh$ and $e^{-}e^{+} \rightarrow \nu\bar{\nu}h$ respectively. In advance, we should confirm that the 1-loop correction does not buried in this error. In the left figure, the $\delta_{\text{NLO}}^{\text{SM}}$ is estimated to be $-(6 \sim 9)\%$ in entire region and it is larger than the error. Similarly, in the right figure, $\delta_{\text{NLO}}^{\text{SM}}$ is estimated to be $-4.5 \sim +1.5\%$ in entire region and this value is larger than the error.

From the results we figure out that the 1-loop correction is necessary for reliable theoretical predictions in both processes.

Table 3: The SM parameters used in this report.

u -quark mass	$2.0 \times 10^{-3}\text{GeV}$	d -quark mass	$5.0 \times 10^{-3}\text{GeV}$
c -quark mass	$1.0 \times 10^{-3}\text{GeV}$	s -quark mass	$100.0 \times 10^{-3}\text{GeV}$
t -quark mass	173.5GeV	b -quark mass	$4.75 \times 10^{-3}\text{GeV}$
W boson mass	80.4256GeV	Z boson mass	91.187GeV
higgs mass	125.1GeV	QED fine structure constant	1/137.036

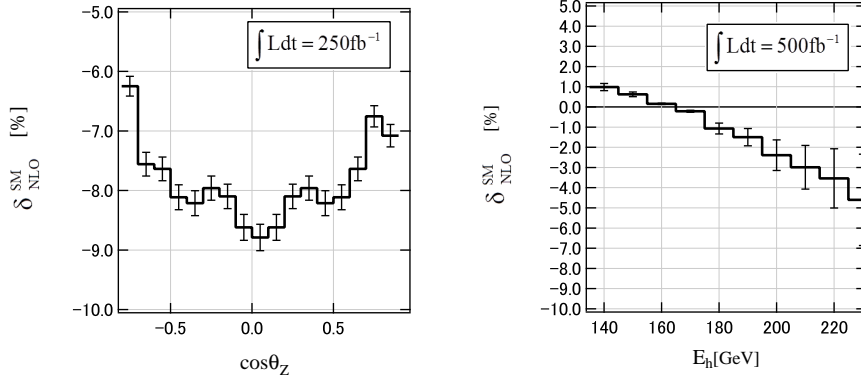


Figure 3: The correction ratio $\delta_{\text{NLO}}^{\text{SM}}$. $e^-e^+ \rightarrow Zh$ with $(\sqrt{s}, L) = (250 \text{ GeV}, 250 \text{ fb}^{-1})$ (left), $e^-e^+ \rightarrow \nu\bar{\nu}h$ with $(\sqrt{s}, L) = (500 \text{ GeV}, 500 \text{ fb}^{-1})$ (right).

4.2 The MSSM contribution

Figure 4 shows the 1-loop corrected angular distribution of Z , $d\sigma/d\cos\theta_Z$ (left) and the ratio δ_{susy} in (4) (right) for the process $e^-e^+ \rightarrow Zh$. From the left figure, we find that the both the SM and the MSSM 1-loop contributions are negative and they are satisfied the relations,

$$\frac{d\sigma_{\text{1loop}}^{\text{SM}}}{d\cos\theta_Z} \lesssim \frac{d\sigma_{\text{1loop}}^{\text{set1}}}{d\cos\theta_Z} \lesssim \frac{d\sigma_{\text{1loop}}^{\text{set2}}}{d\cos\theta_Z} \lesssim \frac{d\sigma_{\text{1loop}}^{\text{set3}}}{d\cos\theta_Z} < \frac{d\sigma_{\text{tree}}}{d\cos\theta_Z}. \quad (17)$$

In the right figure, the δ_{susy} are estimated to be 1.17~1.25% at $\cos\theta_Z = 0$. In the entire region these ratios are larger than the statistical error assuming planned luminosities at the ILC. It means that the 1-loop contribution of the MSSM could be measured at $\sqrt{s} = 250\text{GeV}$. Also, the set 1 will be possibly distinguished from set 2 and set 3.

Figure 5 shows the 1-loop corrected energy distribution of higgs (left) and δ_{susy} (right) in $e^-e^+ \rightarrow \nu\bar{\nu}h$. The left (right) figure shows differential cross section $d\sigma/dE_h(\delta_{\text{susy}})$. In the left figure the SM and MSSM 1-loop contribution are indistinguishable at a glance. However, δ_{susy} are estimated to be 1.5~1.7% and they are larger than the statistical error assuming 500 fb^{-1} in the entire region. It means that the 1-loop contribution of the MSSM could be measured at $\sqrt{s} = 500 \text{ GeV}$. Three proposed sets can not be distinguished each other at least assuming the planned luminosities at the ILC. The precision measurements of the higgs production processes at the ILC will bring us important information on the heavy particles through the virtual 1-loop effects.

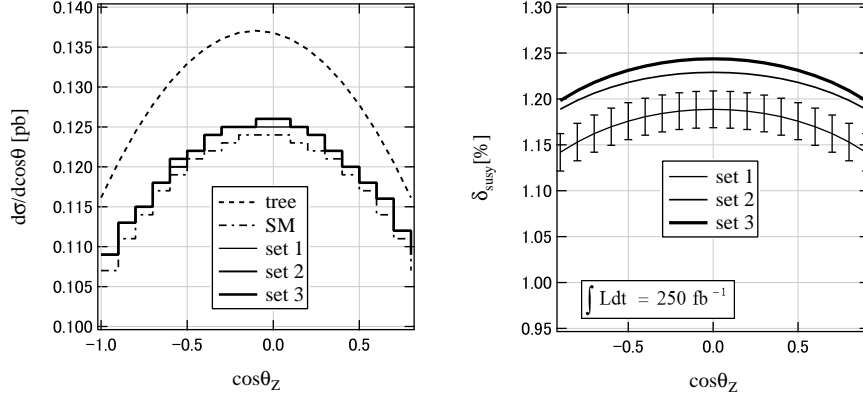


Figure 4: The angular dependence $d\sigma/d\cos\theta_Z$ (left), δ_{susy} (right) at $\sqrt{s} = 250$ GeV in $e^-e^+ \rightarrow Zh$. The error bars mean the statistical error assuming $L = 250 \text{ fb}^{-1}$.

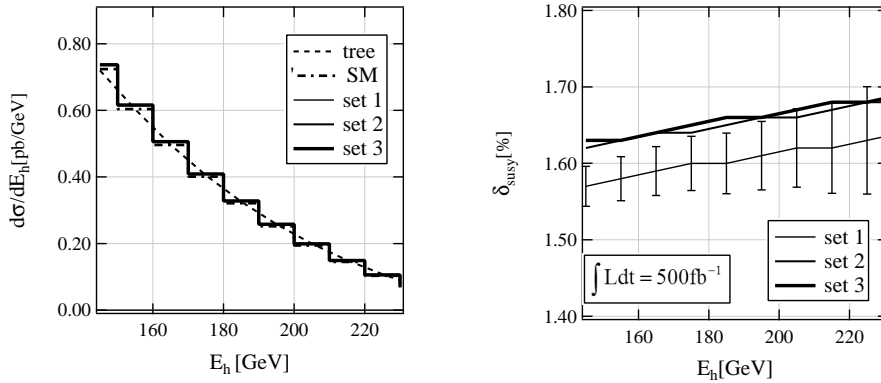


Figure 5: The energy dependence $d\sigma/dE_h$ (left), δ_{susy} (right) of higgs at $\sqrt{s} = 500$ GeV in $e^-e^+ \rightarrow \nu\bar{\nu}h$. The error bars mean statistical error assuming $L = 500 \text{ fb}^{-1}$.

5 Summary and conclusions

We investigated the indirect effects of the MSSM at the ILC. We focused on the center of mass energies of 250 GeV and 500 GeV in the processes $e^-e^+ \rightarrow Zh$ and $e^-e^+ \rightarrow \nu\bar{\nu}h$, respectively. We selected the mass spectra of the MSSM which are consistent with the observed mass of higgs, the thermal relic density of the dark matter, the low energy experiments and the LHC bounds of sparticles. The parameter sets proposed in our calculations have the squarks and the gluino with masses of 1.5, 5.0, 10.0 TeV and the sleptons and gauginos with masses less than 0.5 TeV. With using our developed GRACE system, we calculated the 1-loop corrected cross sections of the processes $e^-e^+ \rightarrow Zh$ and $e^-e^+ \rightarrow \nu\bar{\nu}h$ at the ILC. For the analysis of latter process, we adopted the equivalent W -boson approximation.

We confirmed that both the SM and the MSSM 1-loop correction is necessary for the accurate theoretical predictions at the ILC. We found that the 1-loop effects of MSSM are verifiable both at 250 GeV and 500 GeV. Moreover the difference between set 1 and set 2 and 3 will be possibly observed with $e^-e^+ \rightarrow Zh$ at $\sqrt{s}=250\text{GeV}$.

References

- [1] S. P. Martin, Adv. Ser. Direct. High Energy Phys. **18**, 1 (1998), hep-ph/9709356v7 (2016).
- [2] The ATLAS collaboration, JHEP., **1712**, 085 (2017).
- [3] The CMS collaboration, Phys. Rev. D, **97**, 032009 (2018).

- [4] H. Baer, T. Barklow, K. Fujii, Y. Gao, A. Hoang, S. Kanemura, J. List, H. E. Logan, A. Nomerotski, M. Perelstein, et al. (2013), arXiv:1306.6352.
- [5] Y. Kouda, T. Kon, Y. Kurihara, T. Ishikawa, M. Jimbo, K. Kato, and M. Kuroda, Journal of Physics Conference Series., **920-1**, 012010 (2017).
- [6] Y. Kouda, T. Kon, Y. Kurihara, T. Ishikawa, M. Jimbo, K. Kato, and M. Kuroda, Prog. Theor. Exp. Phys., **2017-5**, 053B02 (2017).
- [7] M. Jimbo, T. Kon, Y. Kouda, M. Ichikawa, Y. Kurihara, T. Ishikawa, K. Kato, and M. Kuroda, (2017), eConf C16-12-05.4 [arXiv:1703.07671].
- [8] M. Kuroda, T. Kon, Y. Kouda, T. Ishikawa, M. Jimbo, K. Kato and Y. Kurihara. Nuclear and Particle Physics Proceedings., **258-259**, 264 (2015).
- [9] J. Fujimoto, T. Ishikawa, Y. Kurihara, M. Jimbo, T. Kon, and M. Kuroda, Phys. Rev. D, **75**, 113002 (2007).
- [10] J. Yan S. Watanuki, K. Fujii, A. Ishikawa, D. Jeans, J. Strube, J. Tian, H. Yamamoto, Phys. Rev. D, **94**, 113002 (2016).
- [11] J. Cao, C. Han, J. Ren, L. Wu, J. Yang, M. Jin and Y. Zhang, Chin. Phys. C, **40**, 113104 (2016).
- [12] P. W. Johnson, F. I. Olness, and Wu-Ki Tung, Phys. Rev. D, **36**, 291 (1987).
- [13] G. Bélanger, F. Boudjema, J. Fujimoto, T. Ishikawa, T. Kaneko, K. Kato, and Y. Shimizu, Phys. Lett. B, **559**, 252 (2003).
- [14] A. Hoecker and W. J. Marciano, The Muon Anomalous Magnetic Moment, in Particle Data Group, Chin. Phys. C **38**, 090001 (2014); p.649 (updated August 2013), references therein.
- [15] G. C. Cho, K. Hagiwara, Y. Matsumoto, and D. Nomura, JHEP., **11**, 068 (2011).
- [16] A. Ibarra, A. Pierce, N. R. Shah, and S. Vogl, Phys. Rev. D, **91**, 095018 (2015).
- [17] J. Ellis, K. A. Olive, and J. Zheng, Eur. Phys. J. C, **74**, 2947 (2014).
- [18] K. A. Olive, PoS, **PLANCK2015**, 093 (2015).
- [19] T. Becher and M. Neubert, Phys. Rev. Lett, **98**, 022003 (2007).
- [20] The ATLAS Collaboration, Phys. Lett. B, **716**, 1 (2012).
- [21] The CMS Collaboration, Phys. Lett. B, **716**, 30 (2012).
- [22] G. Bélanger, F. Boudjema, A. Pukhov, and A. Semenov, Comput. Phys. Commun., **149**, 103 (2002).
- [23] A. Djouadi, J.-L. Kneur, and G. Moultaka, Comput. Phys. Commun., **176**, 42 (2007).
- [24] The ATLAS collaboration, Eur. Phys. J. C, **78**, 154 (2018).
- [25] The CMS collaboration, JHEP., **1803**, 160 (2018).
- [26] The ATLAS collaboration Phys. Rev. D, **96**, 112010 (2017).
- [27] The CMS collaboration, JHEP., **1712**, 142 (2017).
- [28] J. Fujimoto, T. Ishikawa, M. Jimbo, T. Kaneko, K. Kato, S. Kawabata, T. Kon, M. Kuroda, Y. Kurihara, Y. Shimizu, and H. Tanaka, Comput. Phys. Commun., **153**, 106 (2003).
- [29] F. Boudjema and E. Chopin, Z. Phys., **73**, 85 (1997).
- [30] G. Bélanger, F. Boudjema, J. Fujimoto, T. Ishikawa, T. Kaneko, K. Kato, and Y. Shimizu, Nucl. Phys. Proc. Suppl., **116**, 353 (2003).
- [31] N. Baro and F. Boudjema, Phys. Rev. D, **80**, 076010 (2009).
- [32] W. Hollik and C. Schappacher, Nucl. Phys. B, **545**, 98 (1999).